Visual Abstract

Experimental and numerical investigations of the flexural behaviour of Green - Ultra High Performance Fiber Reinforced Concrete beams under repeated loads

Ayman Abdo, Ramadan Asker, Dina Atef, Sayed Ahmed
University of Zagazig, Egypt
eng_a_abdo@yahoo.com, http://orcid.org/0000-0003-4040-6032
askar_250@yahoo.com, http://orcid.org/0000-0002-2345-6790
dinaatif550@gmail.com, http://orcid.org/0000-0003-2345-6792
sayedahmed.str@gmail.com, http://orcid.org/0000-0002-8272-5114

ABSTRACT. There are various benefits to ultra-high-performance fiber-reinforced concrete (UHPFRC). However, using a lot of cement in this type of concrete has a severe disadvantage since it causes pollution and several environmental concerns. Therefore, another type of concrete that achieves the same superior properties as UHPFRC while using less cement in the mixture should be considered. This research examined replacing cement with fly ash to produce environmentally friendly concrete called Green-UHPFRC. The impact of utilizing G-UHPFRC on the flexural behaviour of thirteen beams was investigated experimentally and numerically under repeated loads. The major parameters of the study were fly ash replacement ratios of 15%, 30%, and 45% and adding steel fiber to mixes with ratios of 1, 2, 3, and 4%. The tested beams were compared to the control beam in their backbone and hysteresis curves, failure load, crack propagation and failure modes, energy dissipation, stiffness degradation, and ductility index. From the results obtained, environmentally friendly concrete (G-UHPFRC) can be produced by replacing cement with fly ash up to 45% and adding 2% steel fiber without affecting the bending performance of beams made of G-UHPFRC compared to those made of UHPFRC.

KEYWORDS. Beams, Flexural, Fly Ash, G-UHPFRC, Repeated load, Steel Fiber.

OPEN ACCESS

Citation: Abdo, A., Asker, R., Atef, D., Ahmed, S., Experimental and analytical investigations of flexural behaviour of Green Ultra-High-Performance Fiber Reinforced Concrete beams under repeated load, 64 (2023) 148-170.

Received: 23.10.2022
Accepted: 06.02.2023
Online first: 11.02.2023
Published: 01.04.2023

INTRODUCTION

Many researchers are working to improve concrete design. As a result of their efforts, a new type of concrete called ultra-high performance concrete has been developed (UHPC). The unique mechanical properties of UHPC allow for creative methods to build, maintain, and renovate concrete structures [1]. As a result of continuous efforts, significant advances in the development of Ultra-High Performance Fiber Reinforced Concrete (UHPFRC) have resulted in extensive application in civil engineering, particularly in recent years. Furthermore, because UHPFRC combinations contain a large proportion of Portland cement, this results in high water temperatures and significant CO2 emissions, both of which are important concerns [2]. The employment of processes and procedures that require less Portland cement in UHPFRC combinations is vitally necessary.

Building materials are the third-largest CO2-emitting industrial sector worldwide. One of the critical sustainability challenges for the next decades is designing and producing concrete with less clinker and inducing lower CO2 emissions than traditional one [3]. So to avoid UHPFRC pollution and its effect on the environment, it is necessary to reduce the proportions of cement in the concrete mix and replace it with other environmentally friendly materials [2]. As a result, further research into using lower amounts of ordinary portland cement (OPC) in UHPFRC mixes is required. Green UHPFRC with a low proportion of Portland cement has been developed by employing fly ash (FA) as replacement material [4]. It has an economical and sustainable effect on the cement and concrete industry [5]. Thermal power plant waste, known as fly ash, negatively influences soil and water, accumulates in landfills, and necessitates correct handling. In addition, recycling plastic trash into useful items is vital because it degrades over a lengthy period, especially polyethylene terephthalate bottles. A workable zero-waste technique for reducing environmental pollution has been developed, which uses fly ash to create a lightweight composite aerogel reinforced with recycled polyethylene terephthalate fiber [6].

The amount of cement in the concrete mix must be reduced to produce green concrete, which is more ecologically friendly and has more benefits than normal concrete [7]. Compared to normal concrete, G-UHPFRC has much greater strength, ductility, and fracture toughness. Although the granular combination with a low water-to-binder ratio (W/B) is optimal, adding steel fibers improves the mix's strength [2]

Green concrete is defined as concrete that includes waste materials, has good performance and life cycle sustainability, and does not cause environmental damage during the manufacturing process. Because the cement industry generates eight to ten percent of global carbon dioxide emissions, it is critical to employ natural pozzolan or waste resources to produce ecologically friendly concrete [8]. Using fly ash and cementitious materials to substitute cement in concrete partially has several environmental and technological benefits, including preserving natural resources and reducing greenhouse gas emissions [8]. UHPFRC usually contains soft materials compared to conventional high-strength reinforced concrete. UHPFRC does not usually contain coarse aggregates more prominent than 6-7 mm in size [7]. Elsayed et al. [9] experimentally and numerically investigated twelve rectangular concrete columns with varying UHPFRC thicknesses, steel fiber size ratios, and reinforcing techniques. UHPFRC is an effective reinforcing technique for improving reinforcement concrete R.C. shafts' strength, torque, stiffness, and longevity. Increases in axial load capacity, moment capacity, and stiffness are proportional to UHPFRC casing thickness and inversely proportional to the deflection ratio.

The usage of UHPFRC in different structural applications such as bridges, piers, impact-resistant structures, and repairing and strengthening works has attracted the research community's attention [10]. Because UHPFRC has a significantly higher compressive strength than regular concrete, its high elastic modulus enables the use of elements with smaller cross-sectional dimensions. Furthermore, the steel fibers' improved flexural and shear capability makes them desirable for use in structural components. Because the use of UHPFRC provides significant advantages in flexural and shear behaviour, most experimental and computational studies have been performed on beam members.

Because of its exceptional compressive strength, the balanced reinforcement ratio for the UHPFRC beam section is significantly greater than that of ordinary and high-strength fibrous concretes [7-9]. Applying fly ash in UHPC mixes has enhanced the compressive strength values over the control mix. The strength of UHPC mixes increased as the percentage of fly ash and curing regime increased, thus achieving a strength of 40 MPa at a curing period of 1 day for all mixes. In addition, the binary combinations of FA achieved a strength of 122.4 MPa at 28 days [11]. UHPFRC enhances stiffness and delays the formation of localized fractures, boosting the resistance and longevity of repaired beams[12]. The bending strength of UHPFRC girders, the effect of reinforcement ratio, and methods of concrete placement are studied[13,14].

The way UHPFRC is packaged has been found to have a significant impact on final-moment capabilities. Yu et al. [15] recently evaluated the effect of different fibers on the bending behaviour of UHPFRC-reinforced beams. The final torque

capacity was found to be unaffected by the fiber shape, but the longer steel fibers significantly increased peak response and ductility. This research resorted to producing a new type of concrete [16], which replaces parts of cement with any solid wastes, such as fly ash, to produce new environment-friendly concrete [4], Green Ultra-High-Performance Fiber-Reinforced Concrete (G-UHP-FRC) the same advantages of UHPFRC, and higher compressive strength [17]. Yang et al. studied the bending design and behaviour of UHPC [18]. However, few experimental test results on the flexural capacity and deflection of UHPC beams at the structural level are available. More information is required to develop and upgrade the methods for predicting the flexural behaviour of steel fiber-reinforced UHPC [18].

Accordingly, few rational methods can predict the flexural behaviour of steel fiber-reinforced UHPC. For example, recommendations for UHPC were proposed by Association Francaise de Ge´ nie Civil (AFGC) [7], the Japan Society of Civil Engineers (JSCE) [19], and Deutscher Anschluss für Stahlbeton (DAfStB)[20]. Yoon and Yoo [15] studied the flexural behaviour of UHPFRC beams with different steel fiber lengths for low reinforcement ratios. There is no consensus [21] on test methods or dimensions of specimens for flexural testing between different test standards; RILEM TC 162-TDF, DIN EN14561, ASTM C1609/C1609M, FIB Model Code, and ASTM C293/ C293M recommend three-point bending tests; JCI SF4, NBN B 15 238, Teutsch and ASTM C1399/C1399M, in contrast, recommends four-point beam tests. Moreover, standards such as ASTM C496/ C496M only focus on tensile and flexural strengths. Additionally, Yoo and Hasgul [2,22] report that the UHPFRC outperformed the non-fiber beam and also beam-column joint in terms of load-carrying capability, post-cracking stiffness, and cracking behavior. However, when the longitudinal reinforcement was deformed, the UHPFRC beams had lower ductility ratios. Studies have been done on how well UHPFRC performs under repeated loading. The behavior of the UHPFRC significantly impacts the structural components [23,24].

According to Sarmiento et al., the amount of loading cycles leads the UHPRFC's elasticity modulus to deteriorate [24]. The impressive mechanical performance of beams under repeated loads is evaluated by Hung et al. and Sarmiento et al. [24,25]. Aldahdooh et al. applied repeated loads in one direction [23].

This study investigates the use of fly ash as a cement replacement in the UHPFRC mix to produce eco-friendly concrete (G-UHPFRC) with the same high characteristics as UHPFRC while lowering the quantity of cement in the mixture, hence minimizing environmental harm. Steel fiber plays an important role in improving the mechanical properties of UHPFRC and in compensating for the deficiency in these properties resulting from reducing the proportion of cement in the mixture. Therefore, the main factors that this research focuses on in its studies are the use of fly ash instead of cement at ratios of 15, 30, and 45%, as well as the effect of using a mixture of corrugated and end-hock steel fibers at ratios of 1, 2, 3 and 4%. A reference mixture was prepared without steel fibers or fly ash, and 12 other mixtures were prepared in three groups, each containing four mixtures. In the first group, fly ash replaces cement by 15% of the cement weight for all mixes in the group, and steel fibers were added to the first mix by 1%, to the second mix by 2%, to the third by 3%, and finally by 4% to the fourth mix. Fly ash was used at 30% in the second group, and fiber was used at 1, 2, 3, and 4% in each mixture. Finally, in the third group, fly ash was used at a percentage of 45% with the use of the previous percentages of fiber in each mixture. To evaluate the flexural behaviour of the beams under the impact of repeated loads, three (100 x 100 x 100) mm cubes and a (100 x 300 x 2000) mm beam were poured from each of the 13 mixtures. The tested beams were compared to the control beam in terms of their backbone and hysteresis curves, failure load, crack propagation and failure modes, energy dissipation, stiffness degradation, and ductility index. A finite element model was constructed to validate the experimental results, considering the proportion of mixes, dimensions of tested beams, boundary conditions, and loading profile.

EXPERIMENTAL PROGRAM

Materials and mixture proportions

In this study, local OPC (type I 52.5 N) [26] was partially replaced with three fly ash class F (FA) percentages (15%, 30%, and 45%). A polycarboxylic-based Superplasticizer (type Sikament 163M complying with ASTM C494) was used to enhance the workability of G-UHPFRC. Two sizes of sand were used: micro-sand (from 0 to 1 mm) and normal sand (with sizes from 1 to 2 mm). Silica fume (SF) was added by 5% of the cement content for all mixes. The chemical and physical properties of OPC, SF, and FA. are listed in Tab. 1. The FA and SF confirmed the high active pozzolanic material requirements according to ASTM C618 [9]. Two types of steel fiber (End hooked and Corrugated steel fiber) having an aspect ratio of 50 are employed[26], each type has 50 % of the percentage added to mixes[27], and their characteristics are shown in Fig. 1 [28] and Tab. 2.

Item	OPC	SF	FA
SiO2	20.1	92.26	62.32
Al2O3	5.62	0.89	23..95
Fe2O3	2.17	1.97	1.33
CaO	62.92	0.49	4.74
MgO	1.14	0.96	2.04
Cl	0.0096	0.009	-
SO3	2.92	0.33	1.25
Na2O	0.3	0.42	-
K2O	0.85	1.31	0.76
LOI	3.84	-	3.12
S.D	3150	2200	2130

Table 1: OPC, SF, and FA Chemical and physical properties. S.D= Specific density (kg/m³).

a. Hooked end b. Corrugated

Figure 1: Shape of used Steel Fibers.

Item	Type	Specific density (kN/m³)	Length (mm)	Diameter (mm)	Aspect ratio	Tensile Strength (MPa)
Hooked End	Round	78	50	1	50	1000-1500
Corrugated	Round	78	50	1	50	1000-1500

Table 2: Physical properties of steel fiber.

Mix design

SCC, HSC, and UHPC are examples of materials where Fuller's grading curve is unsuitable since it produces mixes that are difficult to deal with and have low cement content [29]. Nevertheless, using Andreasen and Andersen's [3] particle packing method, the UHPC grain size distribution may be identified. In this instance, the particle distribution is determined using Eqn. 1, where P(Di) denotes the percentage of all solids with a diameter smaller than the specified diameter Di, Dmax denotes the largest particle diameter, and q denotes the distribution modulus, which varies depending on the type of concrete.

$$P(Di) = \left(\frac{Di}{Dmax} \right)^{q} \quad (1)$$

Based on the particle density employed in the study, the UHPFRC combination was created. By increasing the component material filling densities, the performance of the concrete mixture can be improved. The Andreasen and Andersen equation was modified to create the UHPFRC mixes Funk and Dinger [3], presented:

$$P(D) = \frac{D^{q} - D^{q}min}{D^{q}max - D^{q}min} \quad (2)$$

where P(D) is the fraction of all solids smaller than D, D is the particle size in micrometres, Dmax is the largest particle size in micrometers, Dmin is the smallest particle size in micrometers, and q is the distribution modulus.
Yu et al. [3] the ideal packing distribution of a UHPFRC was found using the modified Andreasen and Andersen model. In this instance, a Least Squared Method (LSM)-based method was developed to find the best combinations that match the target. The compressive strength of optimized and non-optimized concrete mixes is equal when compared using the modified Andreasen and Andersen model, demonstrating that the optimizing procedure may lower the quantity of binder without signicantly affecting concrete strength.[29].

Mixing and curing

All powder and sand fractions are mixed for 10 minutes as part of the mixing technique used in this study to create UHPFRC. After about 70% of the water has been mixed into the mixture of dry constituents for seven minutes, the remaining water and 70% of the superplasticizer are added. The mixing continues for another five minutes, add the remaining 30% of the superplasticizer and continue the mixing for another three minutes. Until the mixture has reached homogeneity. All the beams were cured in water after 24 h at room temperature for normal curing until testing after 28 days.

Group	Mix specimens	Mix ID	C kg	S.F kg	Sand 0-1mm kg	Sand 0-2mm kg	S.P kg	W kg	F kg	FA kg	F %	FA %	Compressive strength Mpa	S.D.
Control	Control	0 FA-0 F	875	43.7	218.7	1054.7	46	184	0	0	0	0	96	5.5
Group 1	Mix 1	15%FA-1%F	744	43.7	218.7	1054.7	46	184	78	131	1	15	101	4.03
	Mix 2	15%FA-2%F	744						156		2		102	3.08
	Mix 3	15%FA-3%F	744						234		3		121	3.6
	Mix 4	15%FA-4%F	744						312		4		134	13.07
Group 2	Mix 5	30%FA-1%F	612	43.7	218.7	1054.7	46	184	78	262	1	30	123	16.2
	Mix 6	30%FA-2%F	612						156		2		128	13.6
	Mix 7	30%FA-3%F	612						234		3		125	8.03
	Mix 8	30%FA-4%F	612						312		4		138	2.12
Group 3	Mix 9	45%FA-1%F	481	43.7	218.7	1054.7	46	184	78	393	1	45	98	11.7
	Mix 10	45%FA-2%F	481						156		2		117	17.5
	Mix 11	45%FA-3%F	481						234		3		90	13.2
	Mix 12	45%FA-4%F	481						312		4		108	12.28

Table 3: Mix content of the tested thirteen beams. C: Cement, SF: Silica fume, S.P.: Superplasticizer, W: water, F: Steel fiber, FA: Fly ash, and S.D.: Standard deviation.

Test Specimens setup

Twelve G-UHPFRC beams with different mixes and one control beam without steel fiber or fly ash were tested under 4-point repeated loads. The dimensions for all beams were (2000 mm x 300 mm x 100 mm). The beams were produced in three groups to study the effect of the different fly ash replacement ratios. The first group of beams was cast with a 15% fly ash replacement ratio. While the second group was produced by a 30% fly ash replacement ratio, the last group of beams included a 45% fly ash replacement ratio. The twelve G-UHPFRC mixes and the control mix are listed in Tab. 3. Three cubes of each mixture were poured to evaluate the compressive strength and obtain an average. The geometric sizes and reinforcement details on a typical test beam are given in Fig. 2a. The R.C. beams were reinforced with two 10 mm diameter steel bars at the top and bottom and 8 mm diameter stirrups spaced at 80 mm. All beams and cubes were treated by the Standard Water Curing method "submerged in water for 28 days" before testing.[23] The four-point loading procedure was performed for the flexural tests of beams using a 350 kN movable hydraulic jack to apply repeated load. The repeated load pattern used in this study is in one direction at the middle of the beam. The repeated load consists of repeated loading and unloading. Each load increments by 5 kN more than the previous cycle. The first load started with a 5 kN rate, went back to zero, and then loaded again with an increasing rate of 5 kN against the last cycle until failure. The load was divided into two equal loads by a spreader beam with 600mm between the loads. Fig. 2 shows the test setup and loading method.

A potentiometric transducer was mounted under the mid-span of the beam to measure the vertical deflection. These beams were used to study the load-deflection behaviour, deflection and curvature ductility, flexural stiffness, flexural moment capacity[10], cracking behaviours at the specific deflection values, and compressive strain.

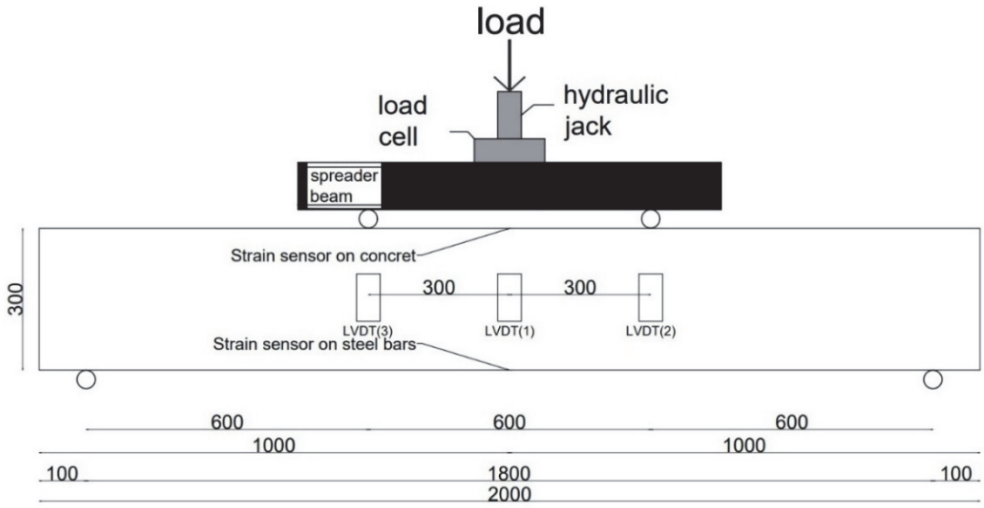

a. Beam geometrical details.

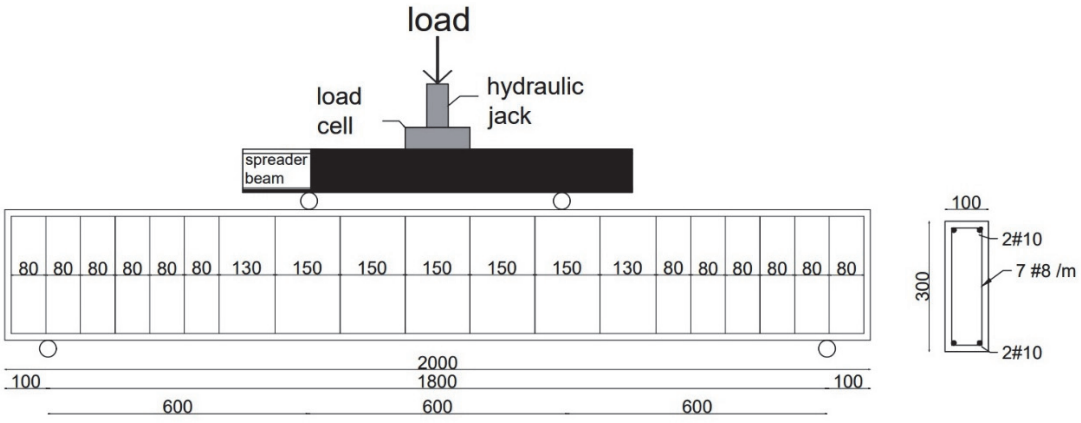

b. Beam reinforcement details.

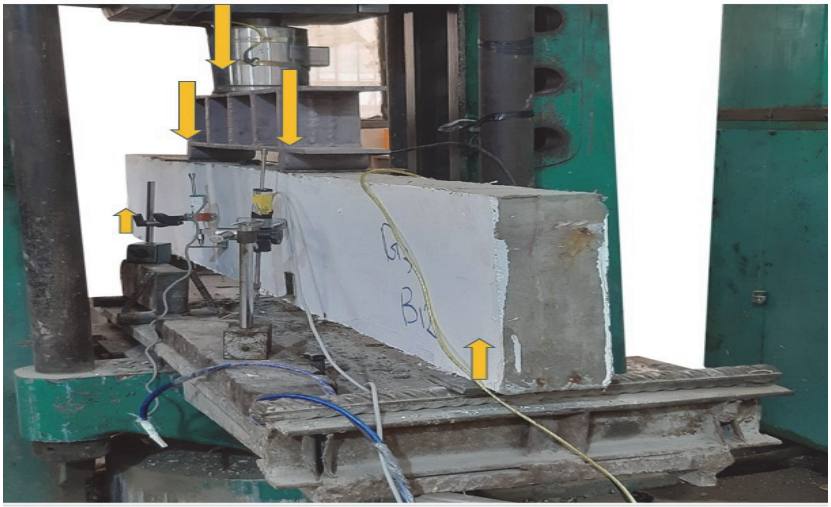

c. Beam setup (four-point load).

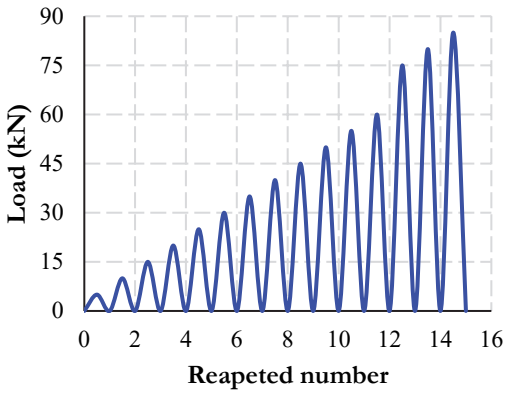

d. Repeated load [23]

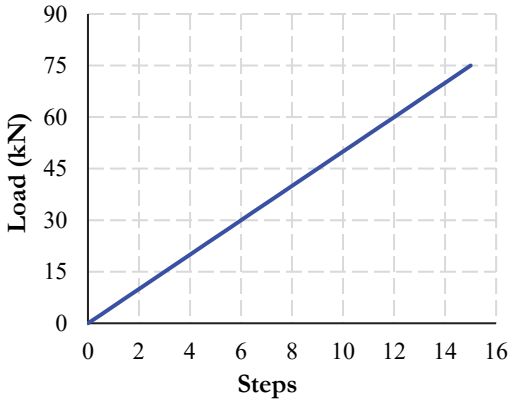

e. Statice load

Figure 2: (a) Beam geometries details, (b) Beam reinforcement details, (c) Beam setup, (d) Repeated load, and (e) Statice load.

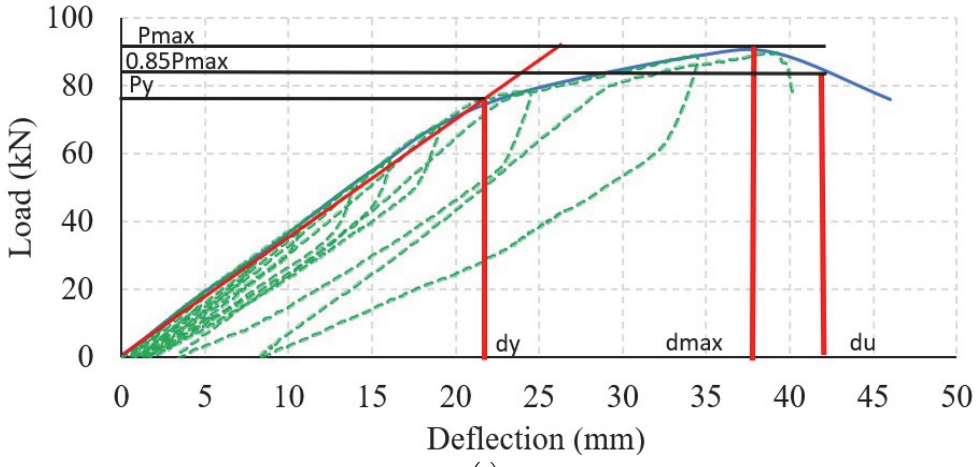

(a)

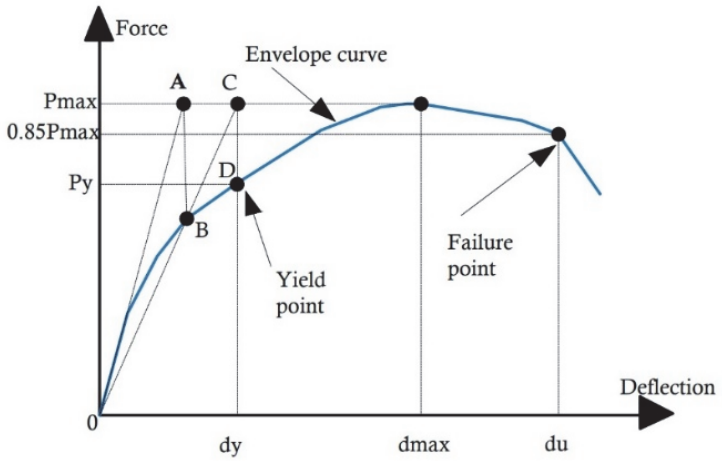

(b)

Figure 3: Yield point from envelope curves (a) and (b).

The specimens were tested in flexure under a four-point flexural repeated load arrangement, as shown in Fig.2. This repeated load was based on concentrated loads in a quasistatic method by producing at least six loading and unloading cycles [23]. Multiple Linear Variable Differential Transformers (LVDTs) placed in the middle of the span were used to measure the deflections of the beams. The result of the first beam was used as a basis to compare the results of the other 12 beams. Fig.3 represents how calculating the yield point is calculated from the envelope curve.

Group	Specimen (I.D.)	Specimen (I.D.)	First Crack load (KN)	Δcr	Yield load (kN)	Δy	Max. load (KN)	Δm	Duc-ratio(μ)	Total accumulated energy dissipation
Control	Control	0 FA-0 F	42	11	66	26	74	45.40	1.75	1201
Group 1	B1	15%FA-1%F	50	14	82	27	90	38.50	1.43	919
	B2	15%FA-2%F	75	19	84	22	89	47.70	2.17	1488
	B3	15%FA-3%F	60	15	80	24	88	39.80	1.66	1293
	B4	15%FA-4%F	65	16	84	21	83	34.10	1.62	1434
Group 2	B5	30%FA-1%F	25	6.5	72	23	85	30.08	1.31	1126
	B6	30%FA-2%F	35	9	76	23	87	31.79	1.38	1994
	B7	30%FA-3%F	50	13	83	24	91	32.79	1.37	1272
	B8	30%FA-4%F	50	13	75	24	92	37.75	1.57	1586
Group 3	B9	45%FA-1%F	70	21	76	26	87	36.43	1.40	1695
	B10	45%FA-2%F	60	17	80	25	90	32.33	1.29	1478
	B11	45%FA-3%F	60	19	77	28	87	35.41	1.26	1398
	B12	45%FA-4%F	75	22	81	25	90	31.33	1.25	1092

Table 4: Results of tested beams.

EXPERIMENTAL RESULTS AND DISCUSSION

The ultimate displacement, peak load, and ductility capacity for negative and positive loading directions were estimated based on the envelope curves of the specimens shown in Fig.4 and Tab. 4. The load-displacement response of reinforcement concrete members could not have a correctly defined yielding point, frequently making determining the yield displacement and estimating the ductility capacity more difficult. This may be due to the nonlinear behavior of the materials (concrete and rebar) or to the failure of separate reinforcement concrete specimen components beginning at different load levels. As a result, it has been standard practice to define parameters affecting reinforcement concrete members' ductility by an idealized bilinear load-displacement relationship[30].

Fig.4 shows the backbone curve of tested beams. Moreover, Tab. 4 presents the data obtained for each specimen in terms of cracking load (*Pcr*), yield load (*Py*), maximum load (*Pm*), and the corresponding displacements ⊿*cr*, ⊿*y*, ⊿*m*, respectively. Additionally, the last two columns present the ductility ratio (*μ*) and the total accumulated energy dissipation. The average increase in *Pm* for beams with a 15 % replacement of cement (Group 1) was 18%, and the reduction in Δm was 7% compared to the control beam. Furthermore, when comparing groups 2 and 3 to the control beam, the average increase in *Pm* was 19%, while the average decrease in ⊿*m* was 26%.

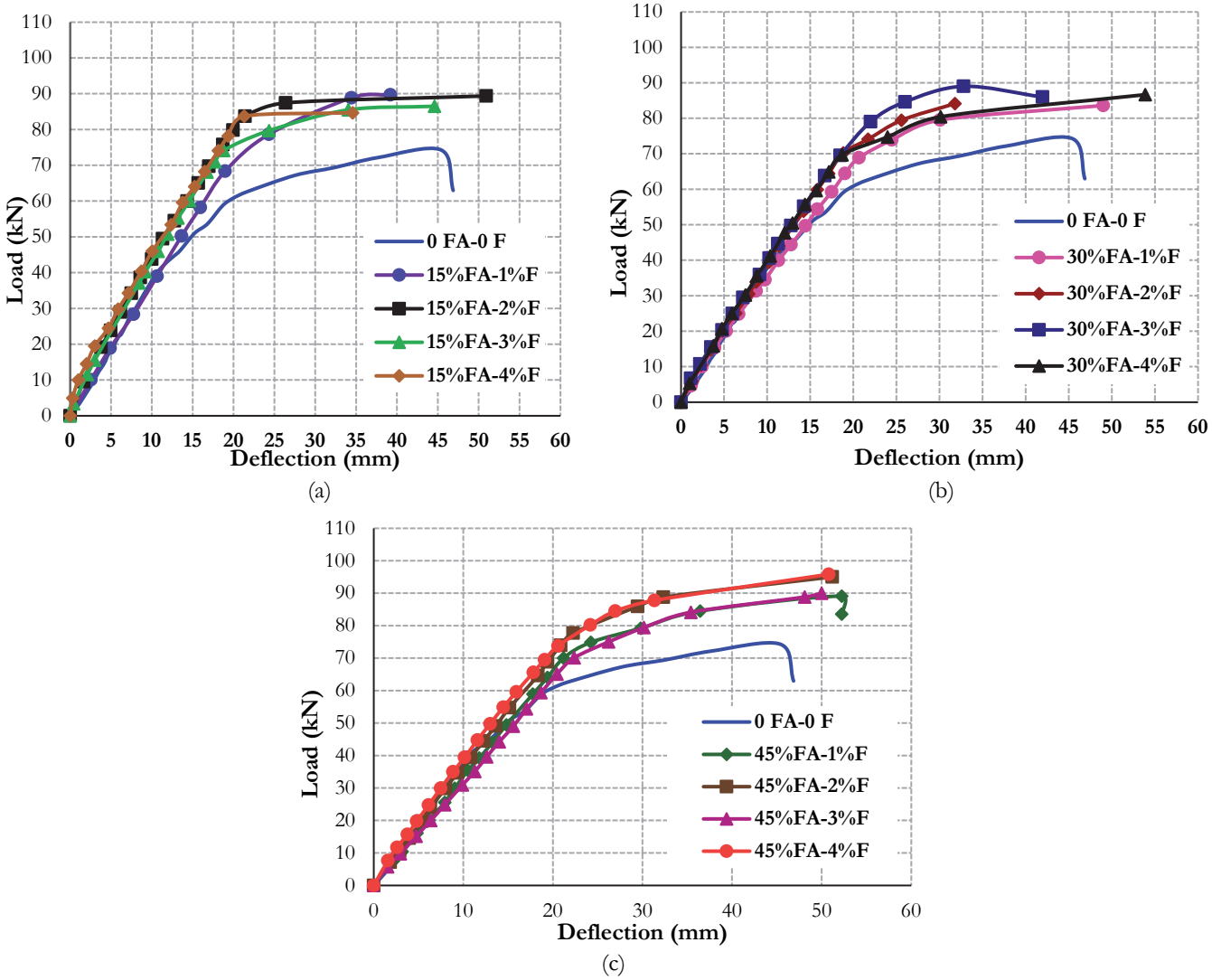

Figure 4: The backbone curves for the tested beams: (a) group1, (b) group2, and (c) group3.

The backbone curves are produced independently for each specimen by linking the envelope points of the hysteretic curve attained in each cycle. As shown in Figs. 4 a,b, and c., the initial stiffness increases with increasing steel fiber volume fraction, where the steel fiber restraints crack preventing their spread and enhancing the initial stiffness.

Fig. 5 shows the influence of steel fiber volume fraction (*Vf*) on the maximum loads (*Pm*) (*Pm* for 15% FA, 30% FA, and 45% FA). The *Pm*. increases by increasing *Vf* up to 2 %, then the value of the *Pm* remains constant up to 3% of *Vf*, and finally, the curve starts to drop where *Vf* reaches 4%. Therefore, it is recommended to use steel fibers with a volume fraction of 2% from an operational and economic perspective. And also Fig. 5 shows the influence of fly ash (*FA*) replacement ratio on the maximum loads (*Pm)* (*Pm* for 1%, 2%, 3%, and 4% of steel fiber volume). The *Pm*. increases with increasing *FA* up to 45 %. Consequently, from an environmental and economic point of view, it is best to use fly ash with a replacement ratio of 45% for cement.

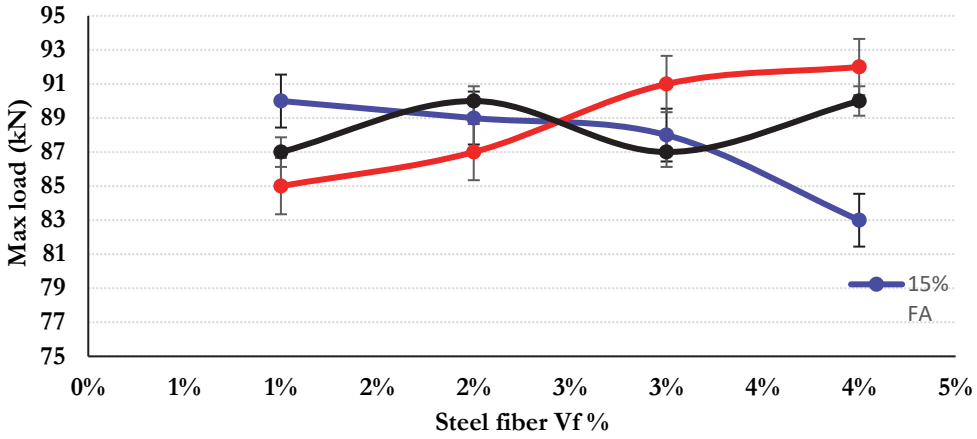

Figure 5: The effect of steel fiber volume fraction and fly ash on the maximum load.

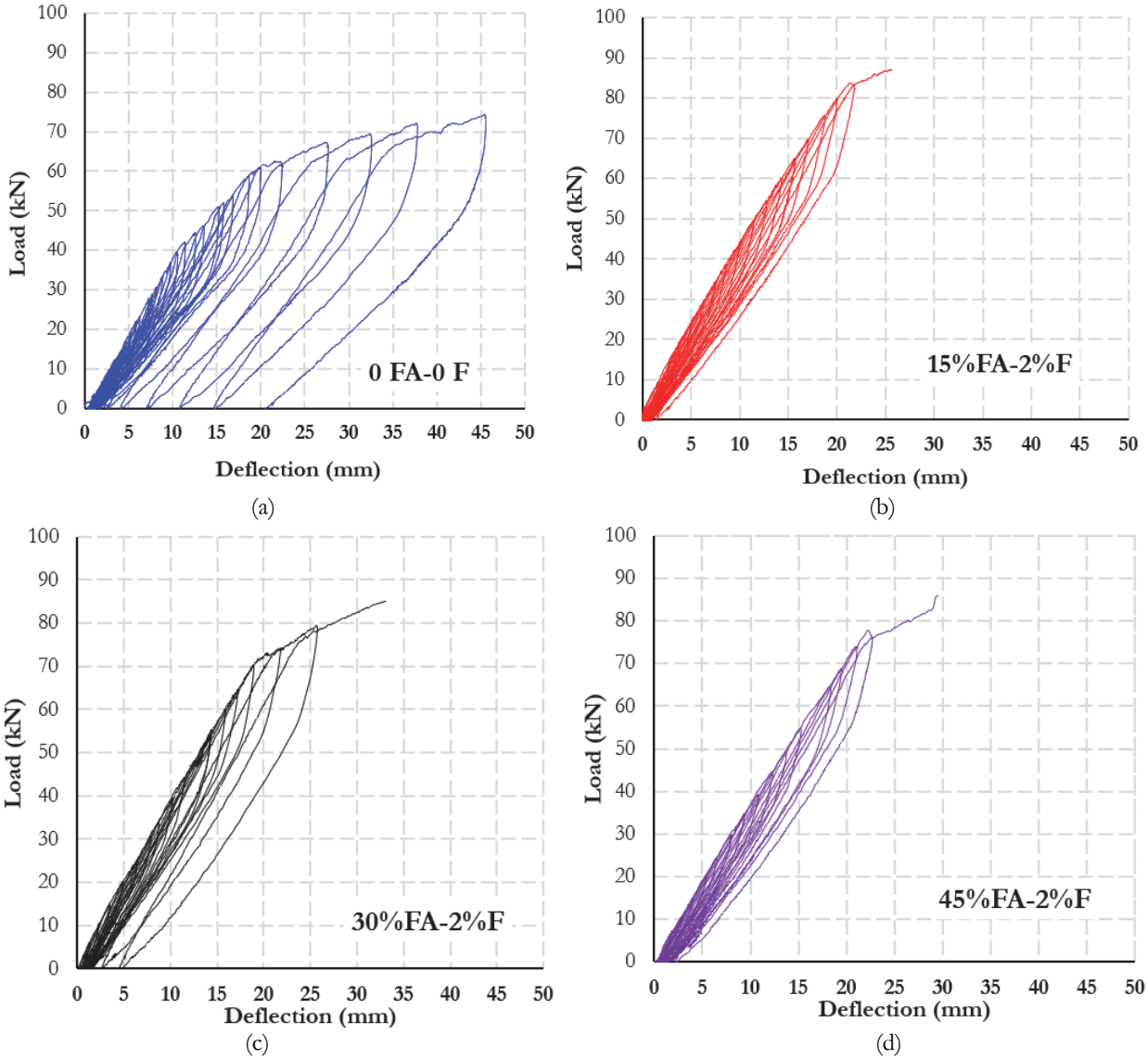

Figure 6: Hysteretic curve of the (a) control beam and beams with steel fiber 2% and fly ash (b) 15%, (c) 30%, and (d) 45%

The load-deflection hysteresis curve under repeated loads is considered the most important attribute in assessing a structural component since it indicates both the ductility and the member's energy dissipation efficiency [23]. Fig. 6 represents the hysteresis curves of tested beams containing 2% of steel fiber, which is considered the optimal ratio of steel fiber in this research. The hysteresis loops of the beams containing steel fiber 2% and fly ash (15% or 30%, or 45%) were larger and more stable than the control beam without stiffness loss. Additionally, the load-deflection relationships for each specimen were linear before cracking, after which point the secant stiffness decreased by increasing load amplitude.

Crack pattern and failure modes

Fig. 7 presents the crack propagation of the tested beams. The failure mode for all tested beams was due to the concrete crushing in the compression zone. The control beam showed the typical flexural crack pattern, with vertical cracks starting in the middle of the span at a load of 42 kN and moving toward the supports as the load increased. The cracks increased in the beam's middle span until the failure load was at 74.3 kN, as shown in Fig.7a.

As shown in Fig. 7b, c, and d, the failure load caused a mix of flexural and shear-flexural cracks in the Group 1 specimens. The first failure load was higher than that of the control beam, as shown in Fig. 5 and Tab. 4, and cracks were localized in the middle of the beam. The steel fiber slows the spread of cracks and gives the beam flexural strength by resisting tensile stresses until the bond between the steel fibers and the concrete breaks, causing the beam to fall suddenly.

According to the observed association between steel fiber and cracks, increasing steel fiber proportion causes a reduction in cracks.

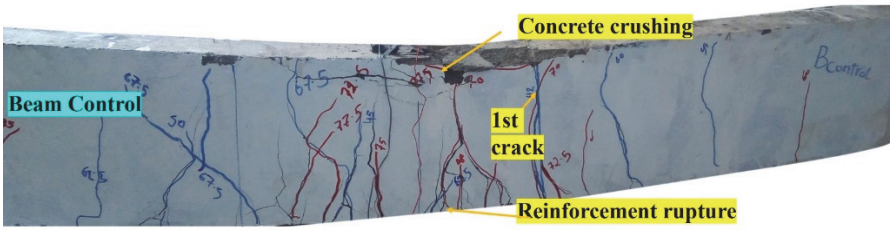

a. Control beam.

b.

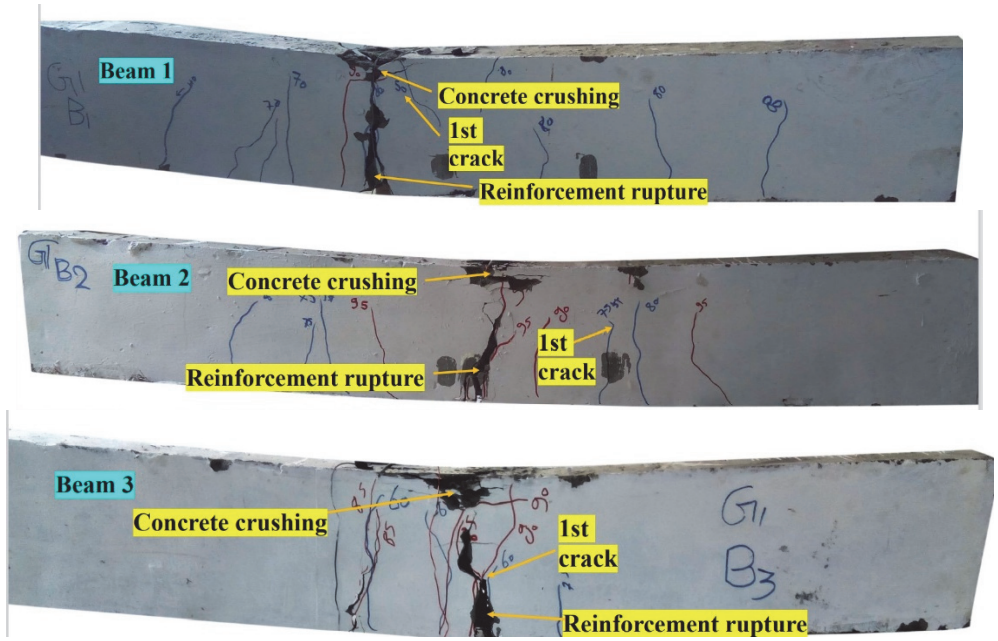

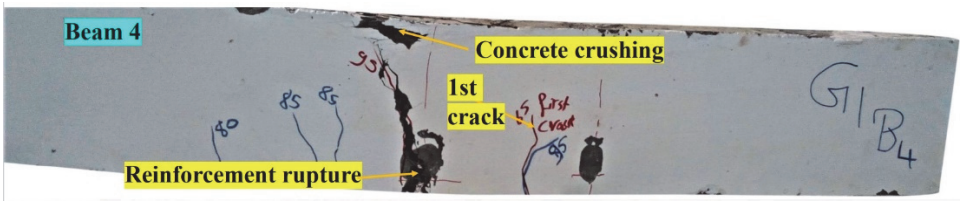

c. Group 1.

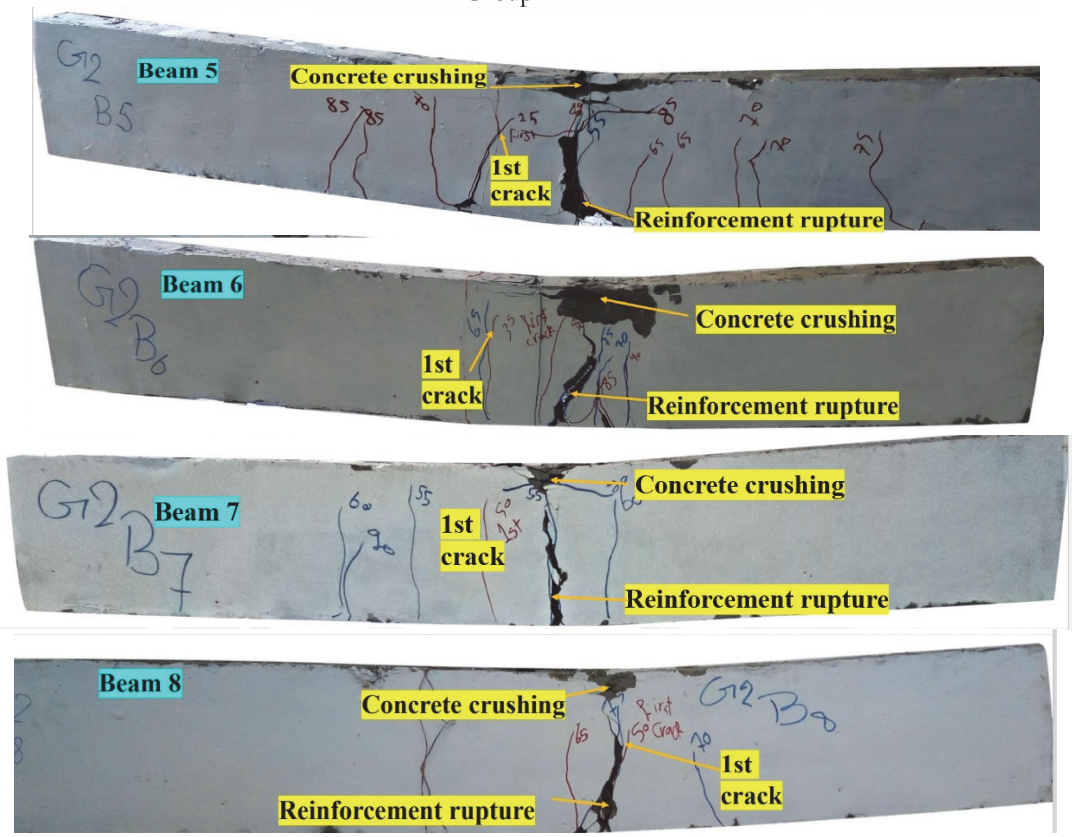

d. Group 2.

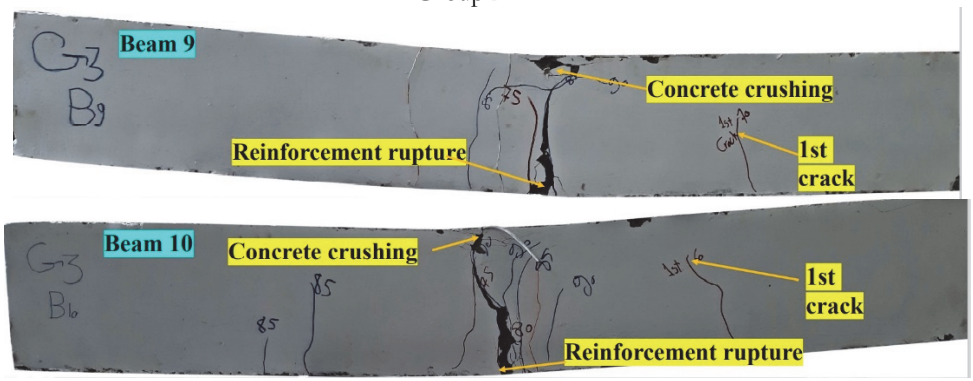

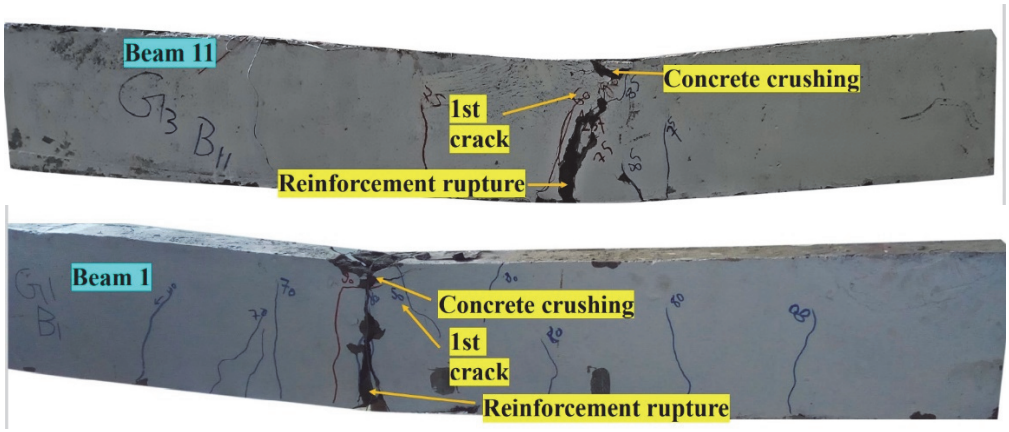

e. Group 3.

Figure 7: Crack propagation and failure modes of tested beams : (a) Control beam, (b) Group 1, (c) Group 2, and (d) Group 3.

DUCTILITY FACTOR

There are many formulas to calculate the ductility factor. In this study, the ductility factor is considered to be the ratio between the maximum deflection of the sample and the yield deflection [31]

$$\mu=\Delta m/\Delta y \quad (3)$$

where Δm is the deflection corresponding to the maximum load and Δy is the yield deflection calculated according to Fig. 3. Fig.8 represents the ductility factor for all tested beams. The beam (15% FA-2%F) has the largest ductility factor; otherwise, the beam (45% FA-4%F)has the lowest value. Fig. 9 shows the influence of steel fiber volume fraction (*Vf*) on the ductility factor (μ) (μ for 15% FA, 30% FA, and 45% FA). The μ decrease with increasing *Vf*. The μ decreased by 21%, 8%, 18%, and 15% for beams containing 1%, 2%, 3%, and 4% of fiber, respectively. This means that beams with a fiber content of 2% have the largest ductility factor. And also Fig. 9 shows the influence of fly ash (*FA*) replacement ratio on the ductility factor (μ) (μ for 1%, 2%, 3%, and 4% of steel fiber volume). The μ decreases with increasing *FA* up to 45 %.

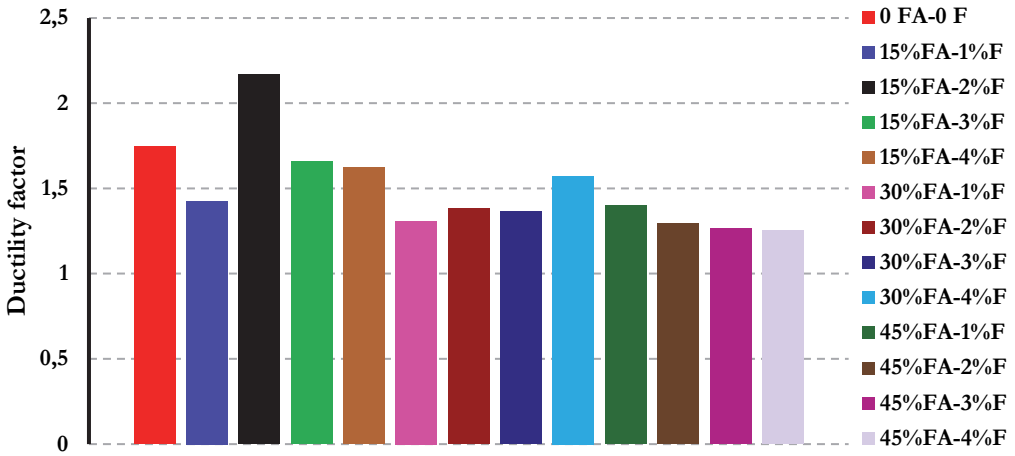

Figure 8: Ductility factor for all specimens.

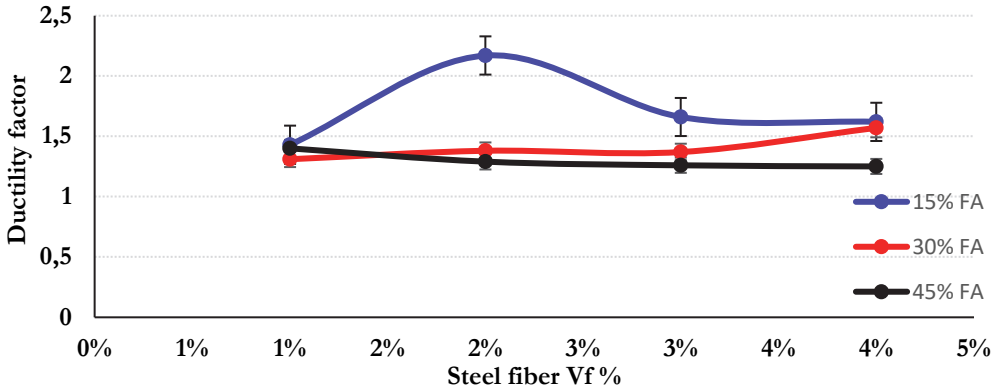

Figure 9: The effect of steel fiber and fly ash volume fraction on the ductility factor.

STIFFNESS

Repeated loading causes micro-cracks inside the beams by loading and unloading. Thus, the concrete beam is subjected to deformations, which decrease the structural element's strength and increase the beam's level of damage, reducing stiffness [30]. In this study, to calculate the stiffness degradation per cycle, the line between the maximum load at the end of the cycle and the load at the beginning of this cycle was drawn, and then the slope of this line was calculated [23].

$$K = P/Ds \ (kN/mm) \quad (4)$$

where P is the maximum load of the cycle, and Ds is the average of the displacement at maximum load and displacement at the beginning of the loading curve. Fig.10 shows the stiffness degradation of all tested beams. In the first cycle, the stiffness increases by increasing the steel fiber volume fraction up to 3% and increases with fly ash to 15%, then decrease by increasing the fly ash replacement ratio up to 45%. Fig. 11 shows the influence of steel fiber volume fraction (*Vf*) on the stiffness for the first cycle (*K*) (*K* for 15% FA, 30% FA, and 45% FA). The *K* increases with increasing *Vf* up to 3%, then the *K* drops at *Vf* equals 4%. The *K* increased by 25%, 58%, 93%, and 63% for beams containing 1%, 2%, 3%, and 4% of fiber, respectively. And also Fig. 11 shows the influence of the fly ash (*FA*) replacement ratio on the stiffness for the first cycle (*K*) (*K* for 1%, 2%, 3%, and 4% of steel fiber volume). The *K* increases with using *FA* by 15 %, then the *K* decreases with increasing *FA* up to 45 %. It can be concluded that beams with a 3% fiber content and a 15% fly ash content have the highest stiffness at the first cycle when compared to other beams.

ENERGY DISSIPATION

The total area under the load-deflection envelope curve for the specimen up to failure was considered the total energy dissipation for the beam. The energy dissipated per cycle equals the area under the load-deflection curve for this cycle.[32]. Fig.12 represents the total energy dissipation for all specimens. The specimens with *FA* of 30% and *Vf* of 2% have the largest total energy dissipation, while those with *FA* of 15% and *Vf* of 1% have the lowest total energy dissipation.

Fig. 13 shows the influence of steel fiber volume fraction (*Vf*) on total energy dissipation (*E*) (*E* for 15% FA, 30% FA, and 45% FA). The *E* increases with increasing *Vf* up to 2%, then the *E* drops with increasing *Vf* up to 4%. The *E* increased by 10%, 38%, 14%, and 11% for beams containing 1%, 2%, 3%, and 4% of fiber, respectively. And also Fig. 13 shows the influence of fly ash (*FA*) replacement ratio on total energy dissipation (*E*) (*E* for 1%, 2%, 3%, and 4% of steel fiber volume). The *E* increases with using *FA* up to 30 %, then the *E* decreases with increasing *FA* up to 45 %. From the preceding, it

can be concluded that beams with a 2% fiber content and a 30% fly ash content have the highest total energy dissipation when compared to other beams.

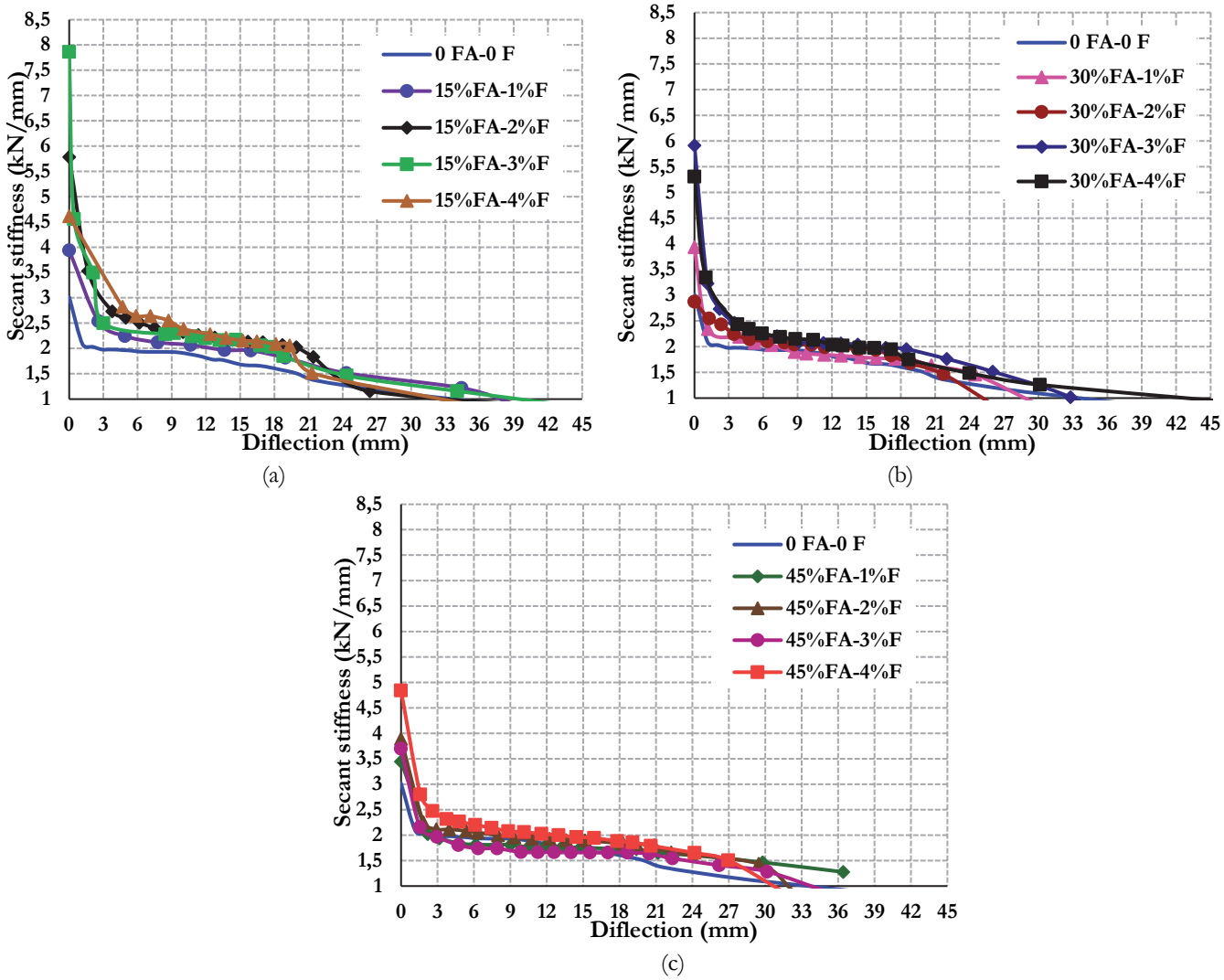

Figure 10: The secant stiffness of tested beams: (a) group1, (b) group2, and (c) group3

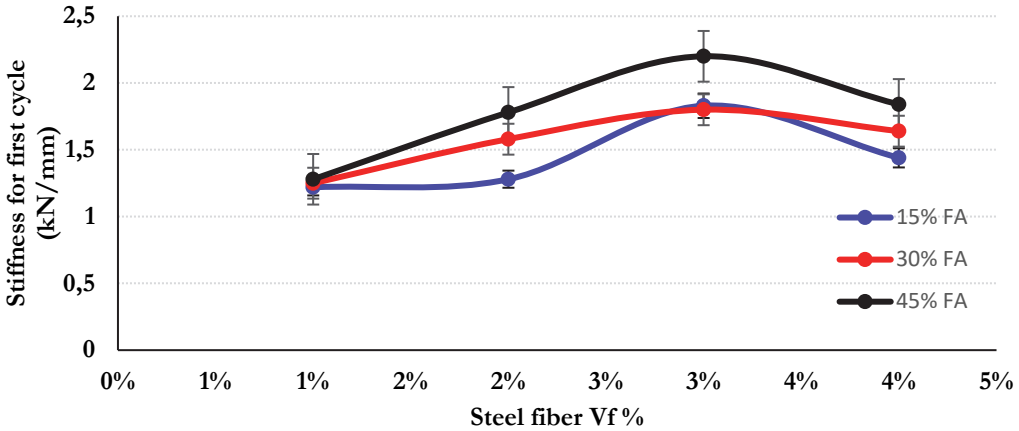

Figure 11: The effect of steel fiber volume fraction and fly ash on the stiffness for the first cycle.

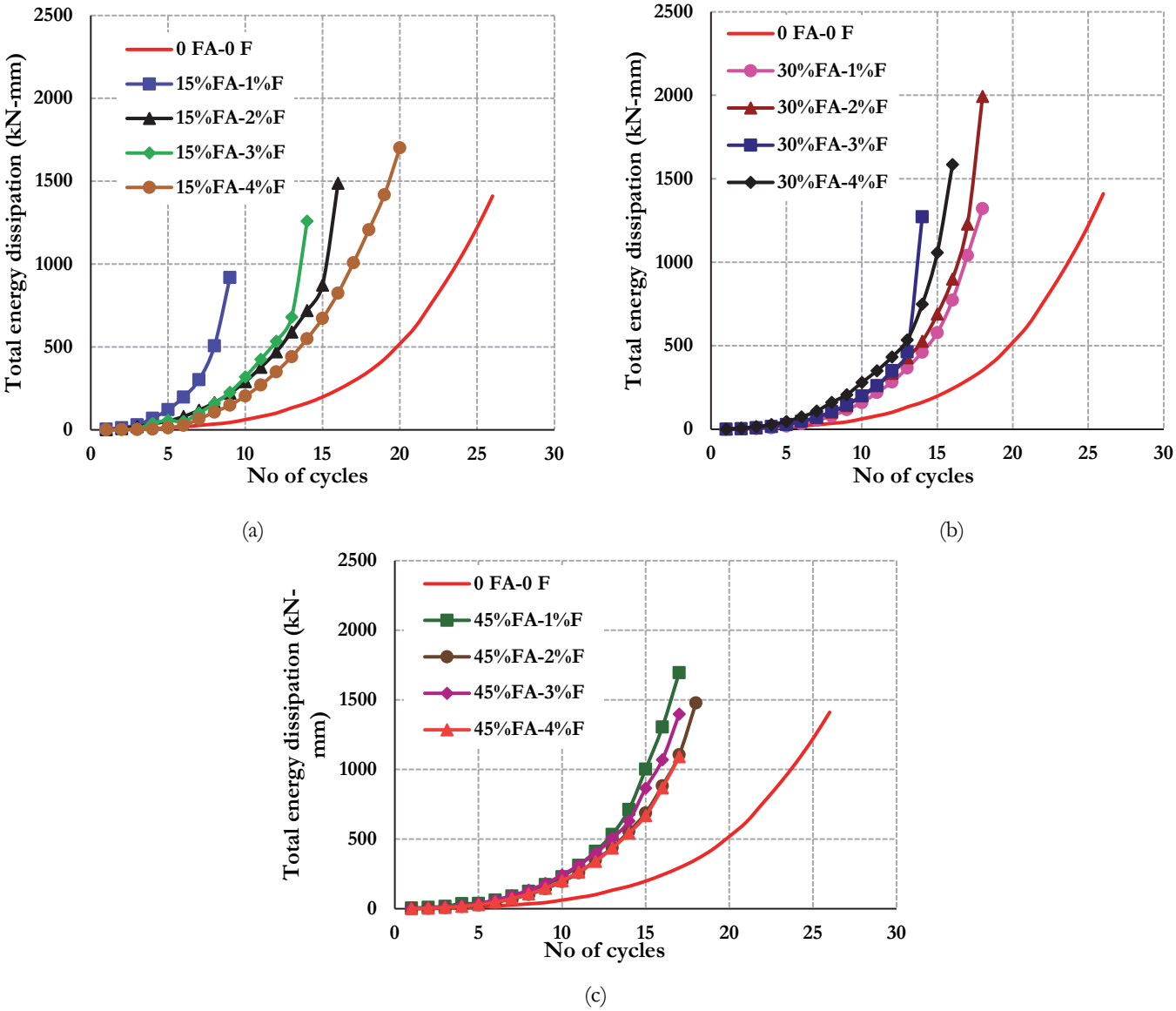

Figure 12: Total energy dissipation for all beams :(a)group1, (b)group2, and (c)group3.

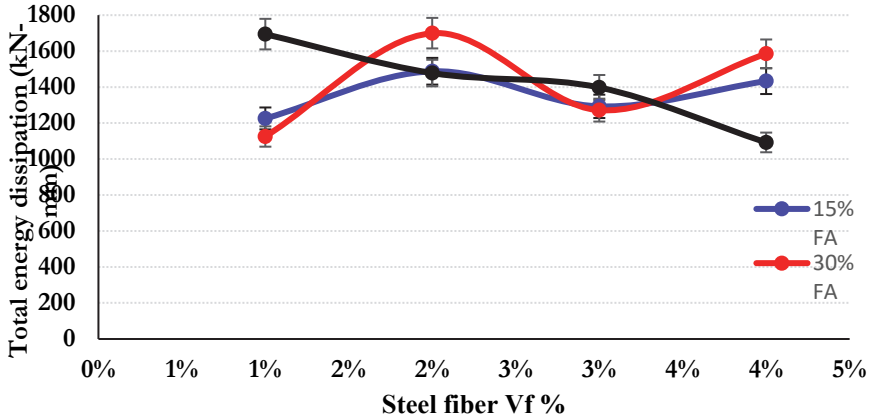

Figure 13: The effect of steel fiber volume fractions and fly ash on the total energy dissipation for all beams.

FINITE ELEMENT MODELLING

A numerical simulation was conducted to model the G-UHPFRC beams to verify the tested beams' experimental findings. A three-dimensional (3D) Finite Element Model (FEM) was constructed by ANSYS 2022R22 [33].

Model construct

The beams were modelled with the same dimensions as those experimentally tested (100 x300x2000)mm Fig. 14. The built FE model is made up of four distinct sorts of elements. A 3-D SOLID65 [34] element was used to represent concrete components that have an eight-node, three-dimensional solid structure with three degrees of freedom at each node translation in the x, y, and z directions used to simulate concrete. The maximum chosen mesh dimension was 15 X 15 mm. LINK180 was a uniaxial tension-compression characteristic so using this element is possible to represent trusses, cables, ties, springs, etc. In this study, stirrups and steel reinforcement are modeled as being encased in a solid mesh. The alternate prefers this choice smeared stiffness potential because it allows for precise placement of the reinforcement while maintaining a relatively coarse mesh for the surrounding concrete medium [35]successfully employed LINK180 to model steel reinforcement in G-UHPFRC, and SOLID 185 was used to model a rigid steel plate[36].

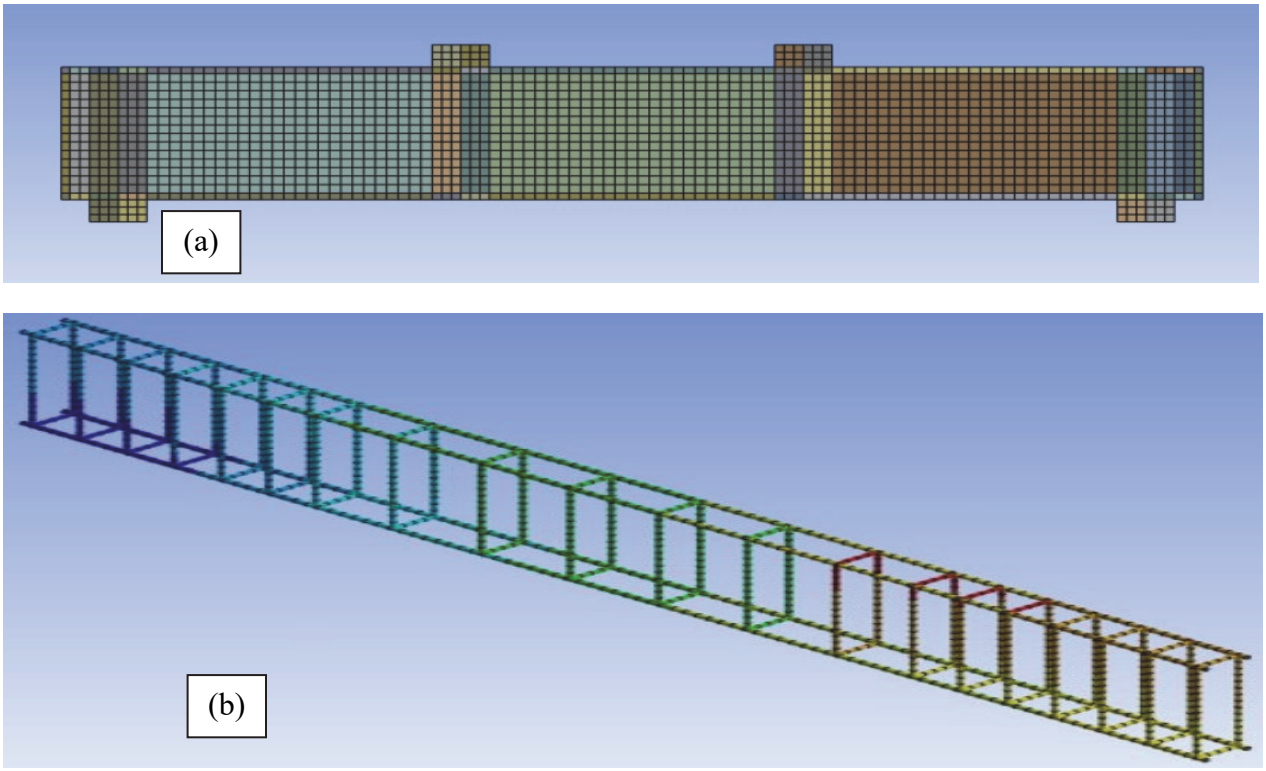

Figure 14: (a) Sample representation of developed FE models., (b) different elements of the beam modelled.

Modelling

The mechanical properties of concrete and steel are from experimental work shown in Tab. 5 and Tab. 6 respectively. The stress versus strain relationships of G-UHPFRC beams was calibrated for experimental testing results and was presented in Fig.15.The linear elastic-plastic behaviour, shown in Fig.16, was used in the FEM for modelling longitudinal steel bars and stirrups.

Group	Specimen (I.D.)	Elastic modulus (GPa)	Poisson's ratio	Compressive strength (MPa)	Tensile strength (MPa)
Control	0 FA-0 F	30	0.2	96	6.3
Group 1	15%FA-1%F	34	0.2	101	7
	15%FA-2%F	34.5	0.2	102	7.2
	15%FA-3%F	35.5	0.2	121	8.2
	15%FA-4%F	39	0.2	134	9.4
Group 2	30%FA-1%F	36	0.2	123	8.3
	30%FA-2%F	37	0.2	128	8.8
	30%FA-3%F	36.5	0.2	125	8.5
	30%FA-4%F	40	0.2	138	10
Group 3	45%FA-1%F	31	0.2	98	6.4
	45%FA-2%F	35	0.2	117	8
	45%FA-3%F	32	0.2	90	6
	45%FA-4%F	34.	0.2	108	7.8

Table 5: The mechanical properties of concrete from experimental work.

Material	Elastic modulus (GPa)	Poisson's ratio	Yield strength (MPa)
Steel bars	210	0.3	500
Stirrups	210	0.3	330

Table 6: The mechanical properties of steel reinforcement from experimental work.

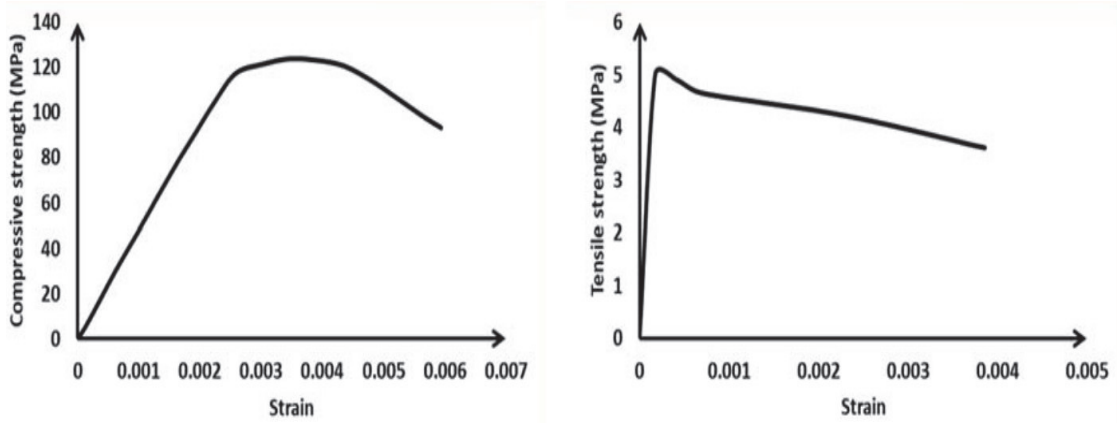

Figure 15: The stress-strain response of G-UHPFRC

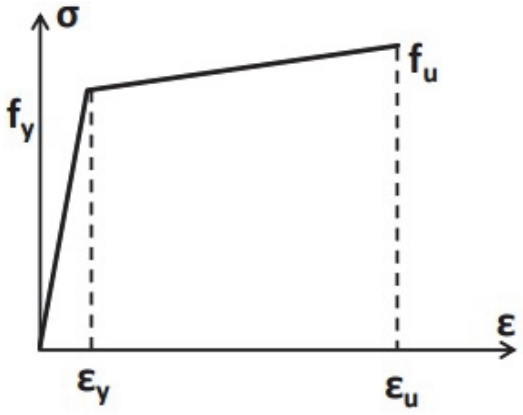

Figure 16: Stress-strain constitutive relationship of steel.

FEM validation

The FEM results, in terms of load-deflection envelope curve, maximum load, and crack pattern, were compared with the experimental ones. Tab. 7 compares the maximum load from the experimental and FEM. analyses, revealing that the FEM could reasonably predict the maximum beam capacity with an average ratio (PFEM/PExp.) of 1.07 and a COV of 0.08. Figs. 17 and 18 represent the verified beams containing 2% steel fiber, considered the optimal steel fiber ratio in this research, fly ash replacement ratio (15%, 30%, and 45%), and the control beam was selected for validation. Results revealed that the FEM could suitably predict the failure mode and crack patterns, as shown in Fig. 17, and the model could simulate the flexural behaviour of G-UHPFRC beams under repeated loading, as presented in Fig. 18. It can be concluded that there is a great agreement between the experimental and numerical results in terms of the maximum load, the shape of the load-deflection envelope curve and the shapes and spread of cracks and the pattern of failure. This increases confidence in experimental results and helps in studying many other parameters numerically.

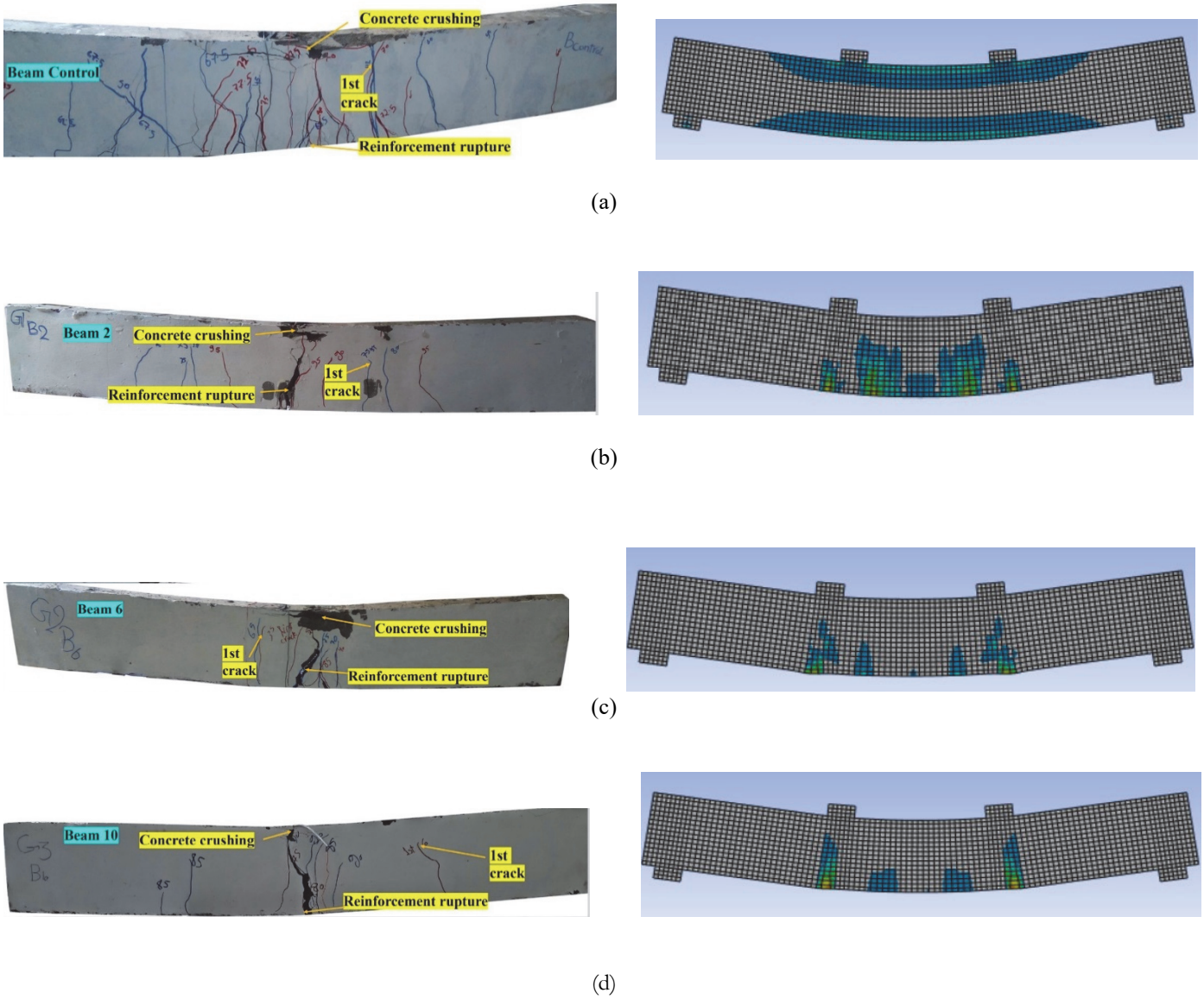

Figure 17: Experimental versus finite element the failure mode and crack pattern of tested beams: (a) control beam, (b) Group1, (c) Group2, and (d) Group3.

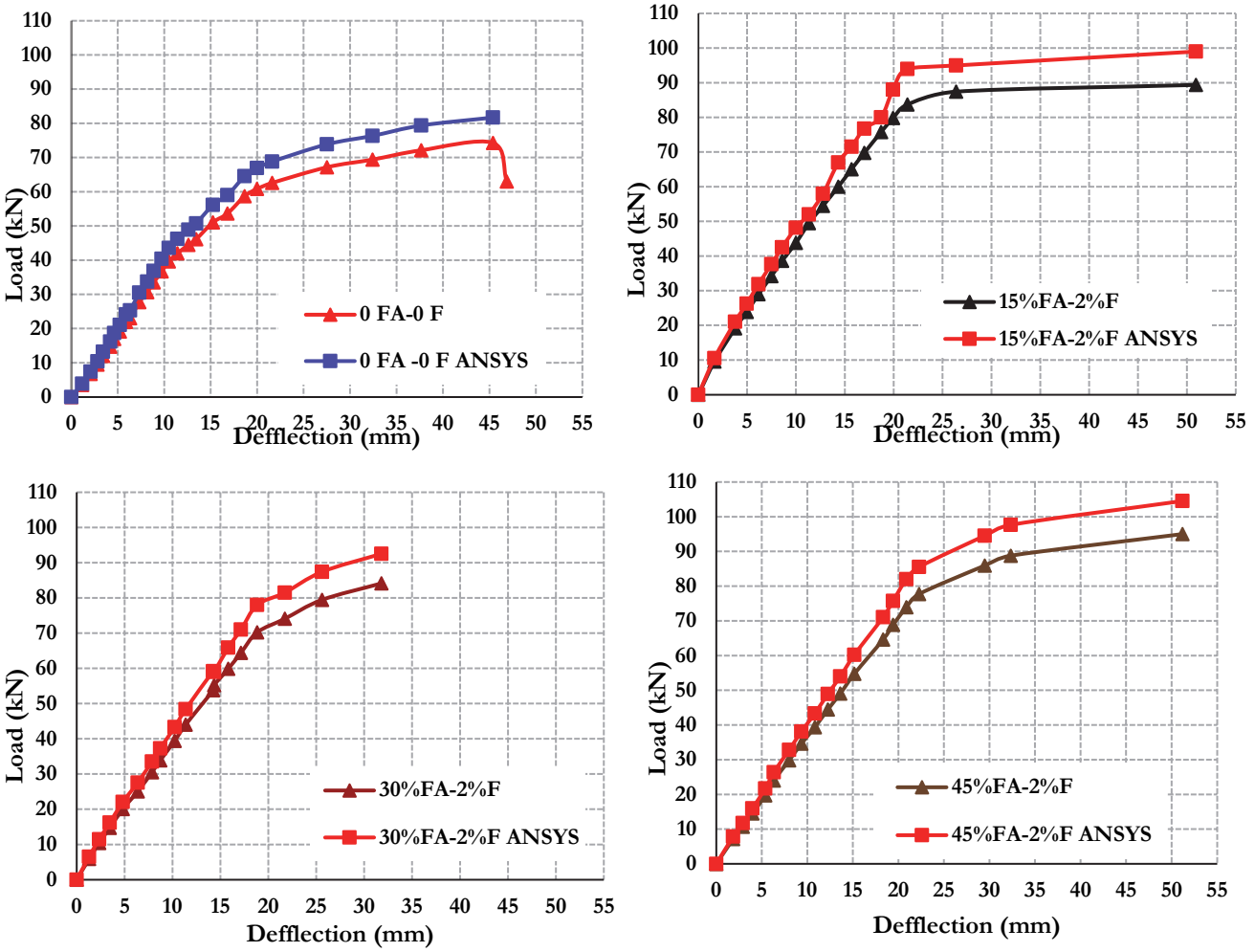

Figure 18: Experimental versus finite element backbone carve at 2% steel fibers.

Group	Specimens ID	FEM. Pm (kN)	Exp. Pm (kN)	P FEM /P Exp.
Control	0 FA-0 F	75.0	74.3	1.01
Group 1	15%FA-1%F	98.7	89.7	1.1
	15%FA-2%F	96.6	89.4	1.08
	15%FA-3%F	86.8	87.7	1.09
	15%FA-4%F	74.7	83	1.09
Group 2	30%FA-1%F	90.4	84.5	1.07
	30%FA-2%F	85.6	86.5	1.03
	30%FA-3%F	95.6	91	1.05
	30%FA-4%F	96.6	92	1.05
Group 3	45%FA-1%F	95.7	87	1.1
	45%FA-2%F	117.0	90	1.03
	45%FA-3%F	92.2	87	1.06
	45%FA-4%F	99.0	90	1.1
Mean				1.07
Coefficient of variation (COV)				0.08

Table 7: FEM results versus experimental results

Conclusions

This research examined replacing cement with different fly ash ratios to produce G-UHPFRC. The impact of utilizing G-UHPFRC on the flexural behaviour of thirteen beams was investigated experimentally and numerically under repeated loads. The major parameters of the study were fly ash replacement ratios of 15%, 30%, and 45% and adding steel fiber to mixes with ratios of 1, 2, 3, and 4%. The tested beams were compared to the control beam in terms of their backbone and hysteresis curves, failure load, crack propagation and failure modes, energy dissipation, stiffness degradation, and ductility index. The following conclusions have been drawn from the analysis of the results:

1. The maximum loads (average of beams containing 15% FA, 30% FA, and 45% FA) increase with increasing Vf up to 2 %, then remain constant up to 3% of Vf, and finally, the curve starts to drop where Vf reaches 4%.
2. The maximum loads (average of beams containing 1%, 2%, 3%, and 4% of steel fiber) increase with increasing FA up to 45 %. Consequently, from an environmental, economic, and operational point of view, it is recommended to use fly ash with a replacement ratio of 45% from cement and steel fibers with a volume fraction of 2%.
3. The failure mode for all tested beams was due to the concrete crushing in the compression zone.
4. The steel fiber slows the spread of cracks and gives the beam flexural strength by resisting tensile stresses until the bond between the steel fibers and the concrete breaks, causing the beam to fall suddenly.
5. According to the observed association between steel fiber and cracks, increasing steel fiber proportion causes a reduction in cracks.
6. The ductility factor (average of beams containing 15% FA, 30% FA, and 45% FA) decreases with increasing Vf. The ductility factor decreased by 21%, 8%, 18%, and 15% for beams containing 1%, 2%, 3%, and 4% fiber, respectively, compared to the control beam.
7. The ductility factor (average of beams containing 1%, 2%, 3%, and 4% of steel fiber) decreases with increasing FA up to 45 %. Consequently, beams with a fiber content of 2% have the largest ductility factor after the control beam.
8. The initial stiffness for the first cycle (average of beams containing 15% FA, 30% FA, and 45% FA) increases with increasing Vf up to 3%, then drops at Vf equals 4%.
9. The initial stiffness increased by 25%, 58%, 93%, and 63% for beams containing 1%, 2%, 3%, and 4% fiber, respectively, compared to the control beam.
10. The initial stiffness for the first cycle (average of beams containing 1%, 2%, 3%, and 4% of steel fiber) increases by using FA by 15 %, then decreases with increasing FA up to 45 %. Consequently, 3% fiber and 15% fly ash content have the highest stiffness at the first cycle compared to control and other beams.
11. The total energy dissipation (average of beams containing 15% FA, 30% FA, and 45% FA) increases with increasing Vf up to 2%, then drops with increasing Vf up to 4%.
12. The total energy dissipation increased by 10%, 38%, 14%, and 11% for beams containing 1%, 2%, 3%, and 4% fiber, respectively, compared to the control beam.
13. The total energy dissipation (average of beams containing 1%, 2%, 3%, and 4% of steel fiber) increases with using FA up to 30 %, then decreases with increasing FA up to 45 %.
14. 2% fiber and 30% fly ash content have the highest total energy dissipation compared to control and other beams.
15. There is a great agreement between the experimental and numerical results in terms of the maximum load, the shape of the load-deflection envelope curve, the shapes and spread of cracks, and the pattern of failure. That increases confidence in experimental results and helps numerically study many other parameters.
16. From the results obtained, environmentally friendly concrete (G-UHPFRC) can be produced by replacing cement with fly ash up to 45% and adding 2% steel fiber without affecting the bending performance of beams made of G-UHPFRC compared to those made of UHPFRC.

References

[1] Khaksefidi, S., Ghalehnovi, M., de Brito, J. (2021). Bond behaviour of high-strength steel rebars in normal (NSC) and ultra-high performance concrete (UHPC), J. Build. Eng., 33, pp. 101592, DOI: 10.1016/j.jobe.2020.101592.

[2] Yoo, D.Y., Banthia, N., Yoon, Y.S. (2016). Flexural behavior of ultra-high-performance fiber-reinforced concrete beams reinforced with GFRP and steel rebars, Eng. Struct., 111, pp. 246–262, DOI: 10.1016/j.engstruct.2015.12.003.

[3] Yu, R., Spiesz, P., Brouwers, H.J.H. (2014). Mix design and properties assessment of Ultra-High Performance Fibre

Reinforced Concrete (UHPFRC), Cem. Concr. Res., 56, pp. 29–39, DOI: 10.1016/j.cemconres.2013.11.002.
[4] Vishwakarma, V., Ramachandran, D. (2018). Green Concrete mix using solid waste and nanoparticles as alternatives – A review, Constr. Build. Mater., , pp. 96–103, DOI: 10.1016/j.conbuildmat.2017.11.174.
[5] Lamine Zeggar, M., Azline, N., Azizi Safiee, N. (2019). Fly ash as supplementry material in concrete : A review, IOP Conf. Ser. Earth Environ. Sci., 357(1), DOI: 10.1088/1755-1315/357/1/012025.
[6] Do, N.H.N., Le, T.M., Tran, H.Q., Pham, N.Q., Le, K.A., Nguyen, P.T.T., Duong, H.M., Le, T.A., Le, P.K. (2021). Green recycling of fly ash into heat and sound insulation composite aerogels reinforced by recycled polyethylene terephthalate fibers, J. Clean. Prod., 322(September), pp. 129138, DOI: 10.1016/j.jclepro.2021.129138.
[7] Pourbaba, M., Sadaghian, H., Mirmiran, A. (2019). A comparative study of flexural and shear behavior of ultra-high-performance fiber-reinforced concrete beams, Adv. Struct. Eng., 22(7), pp. 1727–1238, DOI: 10.1177/1369433218823848.
[8] Suhendro, B. (2014).Toward green concrete for better sustainable environment. Procedia Engineering, vol. 95, Elsevier Ltd, pp. 305–320.
[9] Elsayed, M., Tayeh, B.A., Elmaaty, M.A., Aldahshoory, Y. (2022). Behaviour of RC columns strengthened with Ultra-High Performance Fiber Reinforced concrete (UHPFRC) under eccentric loading, J. Build. Eng., 47, pp. 103857, DOI: 10.1016/J.JOBE.2021.103857.
[10] Turker, K., Hasgul, U., Birol, T., Yavas, A., Yazici, H. (2019). Hybrid fiber use on flexural behavior of ultra high performance fiber reinforced concrete beams, Compos. Struct., 229, pp. 111400, DOI: 10.1016/J.COMPSTRUCT.2019.111400.
[11] Bahedh, M.A., Jaafar, M.S. (2018). Ultra high-performance concrete utilizing fly ash as cement replacement under autoclaving technique, Case Stud. Constr. Mater., 9, DOI: 10.1016/j.cscm.2018.e00202.
[12] Safdar, M., Matsumoto, T., Kakuma, K. (2016). Flexural behavior of reinforced concrete beams repaired with ultra-high performance fiber reinforced concrete (UHPFRC), Compos. Struct., 157, pp. 448–460, DOI: 10.1016/j.compstruct.2016.09.010.
[13] Kahanji, C., Ali, F., Nadjai, A. (2017). Structural performance of ultra-high-performance fiber-reinforced concrete beams, Struct. Concr., 18(2), pp. 249–258, DOI: 10.1002/suco.201600006.
[14] Yang, I.H., Joh, C., Kim, B.S. (2011). Flexural strength of large-scale ultra high performance concrete prestressed T-beams, Can. J. Civ. Eng., 38(11), pp. 1185–95, DOI: 10.1139/l11-078.
[15] Yoo, D.Y., Yoon, Y.S. (2015). Structural performance of ultra-high-performance concrete beams with different steel fibers, Eng. Struct., 102, pp. 409–423, DOI: 10.1016/j.engstruct.2015.08.029.
[16] Habel, K., Viviani, M., Denarié, E., Brühwiler, E. (2006). Development of the mechanical properties of an Ultra-High Performance Fiber Reinforced Concrete (UHPFRC), Cem. Concr. Res., 36(7), pp. 1362–1370, DOI: 10.1016/j.cemconres.2006.03.009.
[17] Aghdasi, P., Ostertag, C.P. (2018). Green ultra-high performance fiber-reinforced concrete (G-UHP-FRC), Constr. Build. Mater., 190, pp. 246–254, DOI: 10.1016/j.conbuildmat.2018.09.111.
[18] Yang, I.H., Joh, C., Kim, B.S. (2010). Structural behavior of ultra high performance concrete beams subjected to bending, Eng. Struct., 32(11), pp. 3478–3487, DOI: 10.1016/j.engstruct.2010.07.017.
[19] Yoo, D.Y., Yoon, Y.S. (2016). A Review on Structural Behavior, Design, and Application of Ultra-High-Performance Fiber-Reinforced Concrete, Int. J. Concr. Struct. Mater., 10(2), pp. 125–142, DOI: 10.1007/s40069-016-0143-x.
[20] Sidodikromo, E.P., Chen, Z., Habib, M. (2019). Review of The Cement-Based Composite Ultra-High-Performance Concrete (UHPC), Open Civ. Eng. J., 13(1), pp. 147–162, DOI: 10.2174/1874149501913010147.
[21] Sadaghian, H., Pourbaba, M., Zeinali Andabili, S., Mirmiran, A. (2021). Experimental and numerical study of flexural properties in UHPFRC beams with and without an initial notch, Constr. Build. Mater., 268, DOI: 10.1016/j.conbuildmat.2020.121196.
[22] Hasgul, U., Turker, K., Birol, T., Yavas, A. (2018). Flexural behavior of ultra-high-performance fiber reinforced concrete beams with low and high reinforcement ratios, Struct. Concr., 19(6), pp. 157715–90, DOI: 10.1002/suco.201700089.
[23] Aldahdooh, M.A.A., Muhamad Bunnori, N., Megat Johari, M.A., Jamrah, A., Alnuaimi, A. (2016). Retrofitting of damaged reinforced concrete beams with a new green cementitious composites material, Compos. Struct., 142, pp. 27–34, DOI: 10.1016/j.compstruct.2016.01.067.
[24] Sarmiento, P.A., Torres, B., Ruiz, D.M., Alvarado, Y.A., Gasch, I., Machuca, A.F. (2019). Cyclic behavior of ultra-high performance fiber reinforced concrete beam-column joint, Struct. Concr., 20(1), pp. 348–360,

DOI: 10.1002/suco.201800025.
[25] Hung, C.C., Chueh, C.Y. (2016). Cyclic behavior of UHPFRC flexural members reinforced with high-strength steel rebar, Eng. Struct., 122, pp. 108–120, DOI: 10.1016/j.engstruct.2016.05.008.
[26] Ahmed, S., Atef, H., Husain, M. (2022). Improvement of mechanical properties of railway track concrete sleepers using ultra high performance concrete (UHPC), Frat. Ed Integrita Strutt., 16(60), pp. 243–264, DOI: 10.3221/IGF-ESIS.60.17.
[27] Li, B., Xu, L., Shi, Y., Chi, Y., Liu, Q., Li, C. (2018). Effects of fiber type, volume fraction and aspect ratio on the flexural and acoustic emission behaviors of steel fiber reinforced concrete, Constr. Build. Mater., 181, pp. 474–486, DOI: 10.1016/j.conbuildmat.2018.06.065.
[28] Mahakavi, P., Chithra, R. (2019). Impact resistance, microstructures and digital image processing on self-compacting concrete with hooked end and crimped steel fiber, Constr. Build. Mater., 220, pp. 651–666, DOI: 10.1016/j.conbuildmat.2019.06.001.
[29] Buttignol, T.E.T., Sousa, J.L.A.O., Bittencourt, T.N. (2017). Ultra High-Performance Fiber-Reinforced Concrete (UHPFRC): a review of material properties and design procedures, Rev. IBRACON Estruturas e Mater., 10(4), pp. 957–971, DOI: 10.1590/s1983-41952017000400011.
[30] Rajabzadeh Gatabi, H., Celikag, M., Akbarzadeh Bengar, H. (2021). Experimental investigation of steel fibers effect on the cyclic behavior of flexural members with moderate ductility, Structures, 34(March), pp. 2530–2543, DOI: 10.1016/j.istruc.2021.09.022.
[31] Palanisamy, D.O.K., Venkatesan, V.P., Arjunan, K., Josephantony, V. (2020). Evaluation of ductility factor for structures subjected to long period of vibration, IOP Conf. Ser. Mater. Sci. Eng., 955(1), DOI: 10.1088/1757-899X/955/1/012023.
[32] Nouri, A., Saghafi, M.H., Golafshar, A. (2019). Evaluation of beam-column joints made of HPFRCC composites to reduce transverse reinforcements, Eng. Struct., 201. DOI: 10.1016/j.engstruct.2019.109826.
[33] Sobhy, A., Nour, L.A., Hassan, H., El-Sisi, A. (2021). Behavior of structural concrete frames with hybrid reinforcement under cyclic loading, Frat. Ed Integrita Strutt., 15(57), pp. 70–81, DOI: 10.3221/IGF-ESIS.57.07.
[34] Schesnyak, L.E. (2019). Modeling of the conjugation of vortex flows with downstream in ANSYS, IOP Conf. Ser. Mater. Sci. Eng., 675(1), DOI: 10.1088/1757-899X/675/1/012026.
[35] Solhmirzaei, R., Kodur, V.K.R. (2017). Modeling the response of ultra high performance fiber reinforced concrete beams, Procedia Eng., 210, pp. 211–219, DOI: 10.1016/j.proeng.2017.11.068.
[36] Fawzy, K., Hassan, H., Madqour, M. (2021). Experimental and analytical investigations of reinforced concrete beams strengthened by different cfrp sheet schemes, Frat. Ed Integrita Strutt., 15(56), pp. 123–136, DOI: 10.3221/IGF-ESIS.56.10.